Mon. Not. R. Astron. Soc. **000**, ??–?? (2006) Printed 19 December 2006 (MN LATEX style file v2.2)

Embedded Stellar Populations towards Young Massive Star Formation Regions I. G305.2+0.2

S. N. Longmore[1,2⋆], M. Maercker[3], S. Ramstedt[3], M.G. Burton[1,4]
[1] *School of Physics, University of New South Wales, Kensington, 2052, Sydney, Australia*
[2] *Australia Telescope National Facility CSIRO, Epping, Sydney, NSW 1710, Australia*
[3] *Institute for Astronomy,Stockholm Observatory, Sweden*
[4] *Armagh Observatory, College Hill, Armagh, BT61 9DG*

ABSTRACT
We present deep, wide-field J, H and Ks images taken with IRIS2 on the Anglo Australian Telescope, towards the massive star formation region G305.2+0.2. Combined with 3.6, 4.5, 5.8 and 8.0μm data from the GLIMPSE survey on the Spitzer Space Telescope, we investigate the properties of the embedded stellar populations. After removing contamination from foreground stars we separate the sources based on their IR colour. We find that the embedded stellar population is spatially offset from the dust emission, although this is most likely caused by the lower completeness limits at longer wavelengths due to strong extended emission in the GLIMPSE images. Stellar density plots reveal that the known embedded cluster in the region, G305.24+0.204, is slightly offset from the dust emission. We discuss the effect of the cluster on the region and argue it may have played a role in triggering the current sites of star formation within the region. There is a gradient in the measured spectral index ($\alpha = d[log(\lambda F_\lambda)]/d[log(\lambda)]$) of stars in the cluster which increases with cluster radius from $\alpha \sim -1.5$ to $\alpha > 1.5$; i.e. the more reddened stars are found at the edge of the cluster. We discuss possible interpretations of this result. Finally, we find that, on average, the younger the source, the closer its projected distance from the current sites of star formation in the molecular cores and examine the possibility that these stars have been ejected from them.

Key words: infrared:stars, stars:early-type, open clusters and associations:general, stars:evolution, stars:formation, stars:pre-main sequence, stars:kinematics.

1 INTRODUCTION

Reprocessing of stellar light by circumstellar material around young stars is observed at infrared (IR) wavelengths as excess emission above that of a blackbody. The extent of the IR excess provides a measure of the amount of circumstellar material and hence an indication of the evolutionary state of the object (e.g. Adams et al. (1987)). Traditionally, the J, H and K bands (1.2, 1.6 and 2.2 μm) have successfully been used to identify IR excess sources (e.g. Lada & Adams (1992)) but recent work including L-band (3.6μm) data has highlighted that IR-excess sources are much more clearly separated using longer wavelengths (Kenyon & Hartmann 1995; Maercker & Burton 2005; Maercker et al. 2006). With large optical depths of material towards the youngest regions, mid-IR observations at high enough spatial resolution to resolve individual sources are required to uncover the most heavily embedded objects (e.g. Longmore et al. (2006)). By combining deep, wide-field, near-IR images of selected regions with catalogued mid-IR data, we aim to identify IR-excess sources, uncover their spatial distribution and investigate the star formation history of the regions. For this first paper, we have chosen a region which has also been studied on the same telescope with near-IR spectroscopy of selected objects (Leistra et al. 2005). Using these, we can calibrate our derived photometric spectral types and so compare results from the automated matching routines to check their accuracy.

1.1 The G305 complex

The $\sim 1.5^\circ \times 1.5^\circ$ region at $l \sim 305^\circ$ within the Scutum-Crux arm of the galaxy, designated G305 by Georgelin et al. (1988), is a large ($\sim$ 100pc in extent) complex of recent and active star formation at a distance of between 3.3 and 4kpc (Leistra et al. 2005). With an age of 3-5 Myr, the complex is one of the most luminous giant HII regions in the galaxy containing in excess of 31 O stars. Clark & Porter (2004) have

⋆ E-mail: snl@phys.unsw.edu.au

recently summarised the global properties of the complex which include two optically revealed clusters, several embedded IR clusters, significant HII emission, many UCHII regions and sites of maser emission (see Clark & Porter (2004) for references and further details). Evidence suggests that the optically revealed clusters (Danks 1 & 2) and associated Wolf-Rayet star (WR 48a) are driving a wind-blown bubble surrounding the entire region, which is responsible for triggering a second generation of star formation - the embedded near-IR clusters - towards the edge of the bubble. This includes the cluster G305.24+0.204, on the NW edge, which contains several late O/early B stars (Leistra et al. 2005) that are only apparent at IR wavelengths. Approximately 3′ (∼ 3pc) SW of this cluster lies an even younger site of massive star formation, heavily embedded in dust and potentially represents a third generation of star formation. Sited near α_{J2000} = 13:11:10, δ_{J2000} = - 62:34:40, it has previously been studied at multiple wavelengths from the near-IR (De Buizer 2003) through mid-IR (Walsh et al. 2001), mm continuum (Hill et al. 2005), mm molecular line (Walsh & Burton 2006), 6.67GHz Class II methanol maser emission (Norris et al. 1993) and cm continuum (Phillips et al. 1998; Walsh 2002). These observations have revealed several distinct sub-regions of star formation (designated by Walsh & Burton (2006)): two ultra-compact (UC) HII regions (G305HII and G305HII(SE)), three cores associated with strong dust emission (G305A, G305B and G305N) and a molecular core offset from the dust (G305SW). These sites of active star formation are co-located within a radius of 1′ (∼1pc), a small fraction of the size of the complex. By studying the surrounding stellar populations we aim to identify the embedded and youngest sources through their IR colours and investigate the recent star formation history.

2 IRIS2 OBSERVATIONS AND DATA REDUCTION

The J, H and Ks-band (1.2, 1.6 and 2.2μm) images were observed using IRIS2[1] (Infrared Imager and Spectrometer 2) on the 3.9m Anglo Australian Telescope (AAT) at Siding Spring Observatory. The Ks band observations were taken on the 25^{th} of July 2002 and the J/H band observations carried out on the 16^{th}-17^{th} May 2006 with seeing of 1 – 1.2″. For each source, a 3 × 3 image grid was created with ∼ 1 ′ offsets from the pointing centre. The integration time at each of the nine grid points was around one minute with 3×20s, 6×10s and 9 × 6s exposures at J, H and Ks respectively. The detector bias was removed at readout time using the Double Read Mode. The data were reduced using the in-house ORAC-DR pipeline with the 'JITTER_SELF_FLAT_KEEPBAD' ORAC-DR[2] recipe to correct for dark current, create flat-field images from star free pixels in the 9 jittered source fields and apply a bad pixel mask to each image. The pipeline then corrects for distortion at the outer edges of the image caused by the slightly curved focal plane. The 9 individual fields of 7.7′×7.7′ were finally aligned and mosaiced together to give a 9.7′×9.7′ field of view, although only the inner 5.7′×5.7′ are covered by all 9 fields. The blind telescope pointing error is estimated to be ∼3″ but absolute coordinates were calculated by comparing non-saturated stars to those in the 2MASS catalogue. Using the *koords* program in the KARMA[3] visualisation package, the image coordinates were matched to better than 0.1 pixel accuracy. We take the error in the absolute coordinates to be the error in the 2MASS catalogue of 0.3″.

The photometry was calibrated from the 2MASS catalogue by plotting the magnitude difference between matched stars as a function of the measured IRIS2 magnitude and the mean offset calculated over a suitable magnitude range (∼12 to 14). The standard deviation in this range is ∼ 0.2 mag but much of this scatter is likely to be due to the difference between the MKO photometric system used by IRIS2 and the 2MASS photometric system[4]. Although converting to the 2MASS photometric system would reduce this scatter, the colour correction terms are not characterised for sources with (J-H) > 1.5, (H-K) > 1 and (J-K) > 2. As we are primarily interested in the sources with reddest colours, the photometry has therefore been left in the MKO system.

Sources were extracted from each of the IRIS2 images using the *daophot* tasks in the IRAF[5] package to produce a J, H and Ks star catalogue. Examination of the residuals after removing the stellar flux from the image shows the stars have been well extracted despite different background levels across the image (due to varying extended emission) and the crowded field. We found 8667, 11762 and 11226 sources at J, H and Ks band respectively with a median photometric error from the automated fitting of ∼0.02 mag. The stars in the individual catalogues with >3σ detections were then matched as outlined in § 4.1 to produce a final IRIS2 JHKs catalogue[6].

2.1 Previous IRIS2 observations

The previous IRIS2 observations carried out by Leistra et al. (2005) were also made using the J, H and Ks band filters with a similar integration time and observation method but were instead focused on the cluster centred at α_{J2000} = 13:11:39.4, δ_{J2000} = -62:33:11. R ≃ 2300 spectra with a 1″-wide slit were also taken toward the cluster. Analysis of the spectra and photometry revealed G305.24+0.204 as an OB association with an O5-O6V star and extinction of A_v ∼12 mags.

3 CATALOGUE DATA

3.1 2MASS - 2 micron All Sky Survey

Using two 1.3m telescopes in Arizona and Chile, the 2MASS survey scanned the entire sky at the J, H and Ks bands (1.25, 1.65 and 2.17μm) (Skrutskie et al. 2006). The survey has a limiting magnitude of 15.8, 15.1, 14.3 ± 0.03 mag at J, H and Ks respectively with a pixel size of 2.0″ and 0.1″ pointing accuracy.

[1] IRIS2 employs a 1024x1024 Rockwell HAWAII-1 HgCdTe infrared detector with a plate scale of 0.4486 ± 0.0002″ per pixel.
[2] see http://www.oracdr.org
[3] http://www.atnf.csiro.au/computing/software/karma/
[4] See http://www.astro.caltech.edu/ jmc/2mass/v3/transformations/
[5] http://iraf.noao.edu/
[6] The final catalogue will be made available on-line.

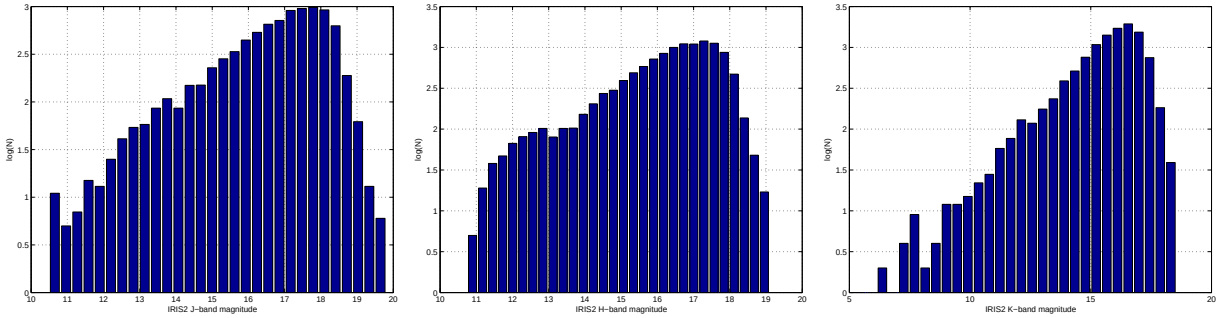

Figure 1. Histograms of the J (left), H (centre) and Ks (right) star magnitudes extracted from the IRIS2 images. The 90% completeness limit from artificial star recovery and maximum measured magnitudes are 18 & 19.8, 17.5 & 19.1, 16.5 & 18.5 at J, H and Ks respectively.

3.2 GLIMPSE - Galactic Legacy Infrared Mid-Plane Survey Extraordinaire

Using the infrared array camera (IRAC) on-board the Spitzer Space Telescope (SST[7]), the GLIMPSE survey has observed the galaxy at 3.6, 4.5, 5.8 and 8.0μm with a 1.2" pixel size between $10^\circ < |l| < 65^\circ$ and $|b| < 1^\circ$ (Benjamin et al. 2003). The photometric accuracy is 0.2 and 0.3 mag for bands 1/2 and 3/4 respectively. The astrometric accuracy of the point source catalogue is $\sim 0.3''$.

4 THE POINT SOURCE CATALOGUE

4.1 Matching sources at different wavelengths

Analysis of source colours relies on the ability to accurately match sources in the catalogues at different wavelengths. With too many sources ($>10^4$) to check manually and crowded stellar fields, there is a potential problem of either matching a source multiple times or mismatching the sources completely. The resulting mismatched sources may replicate the large colour differences of embedded sources and hence contaminate the sample. To test the matching accuracy, we generated and matched synthetic catalogues with known offsets from a list of absolute source positions. In order to ensure a realistic spatial distribution of sources, including over densities due to clustering and under densities due to extinction, the absolute coordinates were taken from the 2MASS PSC of the region. The coordinates recorded in the synthetic catalogues were randomly offset from the absolute values by a 2D Gaussian distribution. Several synthetic catalogues were produced using the known absolute pointing error of the relevant datasets to generate the positional offsets. The sources in the synthetic catalogues were given a unique ID and then matched in the same way as the observed datasets using the *tmatch* routine in the *tables.ttools* package in IRAF. The routine matches every source in the first catalogue with the nearest counterpart in the second catalogue within a user defined matching radius. Comparing the ID of the matched sources in the synthetic catalogues it is possible to unambiguously identify which sources have been matched correctly.

The IRIS2 images were all registered with the same 2MASS image so have a *relative* astrometric uncertainty of $\Delta_{IRIS2} = 0.04''$ (0.1 pixel). The astrometric uncertainty in the 2MASS and GLIMPSE surveys are both quoted as $0.3''$. However, the GLIMPSE survey coordinates were also registered with 2MASS data so the relative uncertainty between the IRIS2 and GLIMPSE catalogues should be considerably less than the assumed error of $\Delta_{IRIS2-GLIMPSE} = 0.3''$. Matching two synthetic catalogues generated with an uncertainty of Δ_{IRIS2}, an equal number of sources and a search radius of 2 pixels, produces a 100% recovery with no confusion due to doubles or mismatches. Matching catalogues generated with an uncertainty of Δ_{IRIS2} but different number of sources also recovers 100% of the sources correctly but includes $\sim$0.05% double sources. With different numbers of sources, the matching order becomes important: matching the catalogue with smaller to larger number of sources produces considerably less doubles but a few more mismatches. However, the number of correctly matched sources is the same, irrespective of the matching order. Varying the matching radius has little effect as long as it is significantly larger than the combined astrometric uncertainty. A matching radius of $1.2''$ was used throughout. We concluded that mismatches do not seriously affect our results.

The final catalogue was generated by matching the catalogues in turn from shortest to longest wavelength. To ensure no red sources were missed, the non-matched sources at the longer wavelength were also appended to the catalogue after each step. After matching the IRIS2 J, H and Ks catalogues to the GLIMPSE PSC using this method, we expect to recover at least 99.8% of the sources correctly with a maximum of 0.1% doubles and 0.12% mismatches.

4.2 Completeness

We used artificial star recovery to investigate the spatial variation in point source senstivity as a function of wavelength. Having calculated the PSF for each image, we inserted a grid of artificial stars of the same magnitude seperated by $30''$ across the image. We then used the same automated finding technique outlined in § 2 to calculate how many of the artificial stars were recovered. The process was repeated by increasing the artificial star magnitudes in steps of 0.5 mag until no more stars were recovered. By recording the largest recovered magnitude at each position and wavelength it was possible to build a three-dimensional picture of the point source sensitivity across the region. The *relative*

[7] http://ssc.spitzer.caltech.edu/

completeness as a function of position was then calculated at each wavelength by subtracting the median completness magnitude at that wavelength from every position.

Figure 2 illustrates the spatial variation in completeness for the J, H and Ks images. The contours show the median-subtracted completeness at -1.5, -1.0 and -0.5 mags highlighting the areas with poorest point source sensitivity. Compared to the three colour image in Figure 5a it is clear that although there is some extended emission, particularly at Ks, the main factors contributing to decreased sensitivity are saturated stars, stellar crowding (e.g. the cluster toward the North-East) and the worse integration time at the edge of the images due to mosaicing. Figure 3 shows similar contours at 3.6 and 4.5μm overlayed on the GLIMPSE images. This time, extended emission is the dominant factor contributing to decreased completeness.

The 90% completeness limit calculated from the artificial star recovery methods above is 18, 17.5 and 16.5 at J, H and Ks respectively. Figure 1 shows a histogram of the calculated J, H and Ks magnitudes. The turnover in the number of stars per magnitude and faintest measured magnitudes are 17.8 & 19.8, 17.3 & 19.1, 16.6 & 18.5 at J, H and Ks respectively. These limiting magnitudes are fainter than those reported by Leistra et al. (2005) of 16, 18 and 18.5 due to confusion towards the cluster, G305.24+0.204, which was the focus of their observations.

4.3 Control Field

In order to compare the sources in the target region with a field star population, a nearby region with no extended emission in either the GLIMPSE or 2MASS images (centred at α_{J2000} = 12:54:10.3 δ_{J2000} = -62:16:12, l=303.25 b=+0.6) was chosen as a control field. All sources in the GLIMPSE and 2MASS catalogues within a 7$'$ radius of this position were matched using the same procedure outlined previously. The total number of sources matched in the control field is 743 compared to the 5456 matched from the GLIMPSE and 2MASS catalogues within the same radius of the target field. This difference in the number of matched sources is not surprising as the control field is farther from the galactic plane. Figure 4 shows the number of sources detected at each wavelength normalised to the number of sources detected at 1.2μm for the target (square) and control fields (circle). In both fields, the number of sources matched up to 4.5μm is similar with a sharp drop at longer wavelengths as most field stars are becoming too faint to detect. This is exacerbated in the target field by the extended emission at 5.8 and 8.0μm.

4.4 Nature of the IR excess sources

We aim to use the catalogue to pick out young stellar objects with excess IR emission through their derived colours. However, these highly reddened colours are not unique to young stellar objects. We are therefore interested in calculating the likely contamination from other astronomical sources with similar colours – primarily evolved stars and background galaxies.

An estimation of the contamination due to background galaxies is possible using results from recent Spitzer observations which have calculated the number count of background galaxies with similar colours to young stellar objects

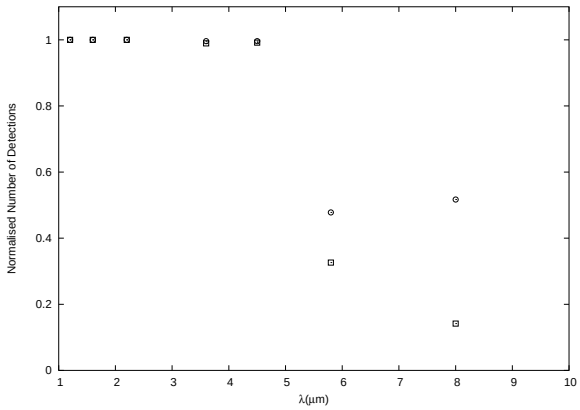

Figure 4. Number of sources detected at each wavelength in the combined 2MASS and GLIMPSE catalogues of the target (square) and control fields (circle) as outlined in § 4.3. The number of sources at each wavelength are normalised to those detected at 1.2μm.

(10<[8.0]<13.5 and [3.6]-[8.0]>1.5) (see Blum et al. 2006, and references therein). Assuming a homogenous spatial distribution with an average value of 245 counts deg^{-2} there are likely to be ∼6 background galaxies within the 9.7$'$×9.7$'$ FOV.

With luminosities of 10^3-10^4L$_\odot$, radiative transfer modelling shows that any asymptotic giant branch (AGB) stars along the line of sight to the edge of the Galaxy will be detected in the IRAC bands (Groenewegen 2006). The same models show that the derived colours, which depend on the mass loss rate of each AGB star, cover the expected colour range for young stellar objects. From photometry alone, it is therefore not trivial to distinguish between AGB stars and young stellar objects. However, with a model distribution of AGB stars in the Galaxy it is possible to predict the expected number of evolved stars within a given field of view. We used the Jackson et al. (2002) model to calculate the number density of AGB stars as a function of Galactic radius and height above the Galactic plane, $|z|$, along our line of sight. By integrating the product of the number density function with discreet volume elements to the edge of the Galaxy, we then derived the expected number of AGB stars along the line of sight. Assuming a Galactic radius of 15kpc, a distance of 8.5kpc to the Galactic centre and using $|z|$=0 (ie looking directly through the Galactic plane) we expect to find ∼0.7 AGB stars along the line of sight. It is therefore unlikely that this region will suffer from evolved star contamination.

5 RESULTS

Figure 5a shows an IRIS2, 3-colour image of the region at near-IR (J, H and Ks) wavelengths and Figure 5b shows the Ks image overlayed with 1.2mm dust continuum emission from Hill et al. (2005) to show the most embedded NIR sources. The image shows lanes of bright extended emission at 2.2μm which are seen as red in the 3-colour image. Figure 6 shows the GLIMPSE images of the region at 3.6 and 4.5μm. The extended emission seen at Ks dominates the 5.8 and 8.0 μm GLIMPSE images, making point source ex-

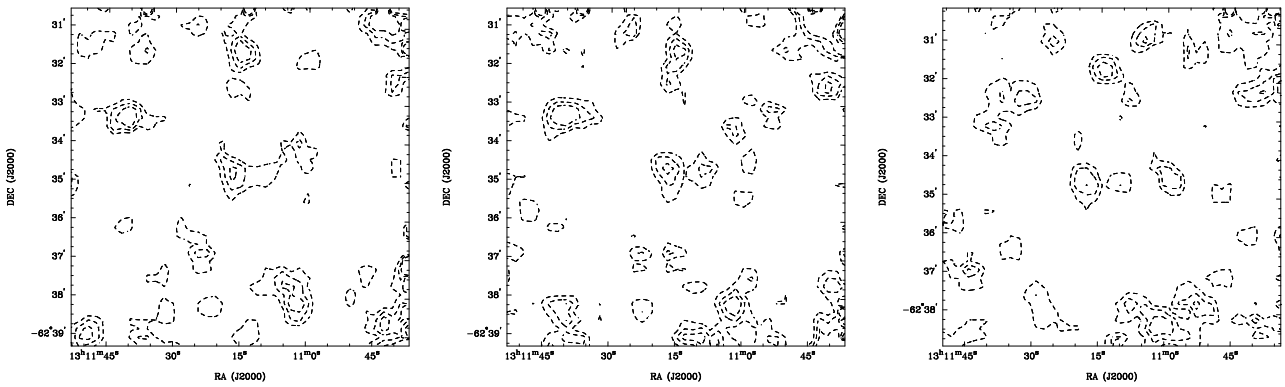

Figure 2. The spatial variation in completeness for the J, H and Ks images calculated as outlined in § 4.2. The contours show the median-subtracted completeness at -1.5, -1.0 and -0.5 mags highlighting the areas with poorest point source sensitivity.

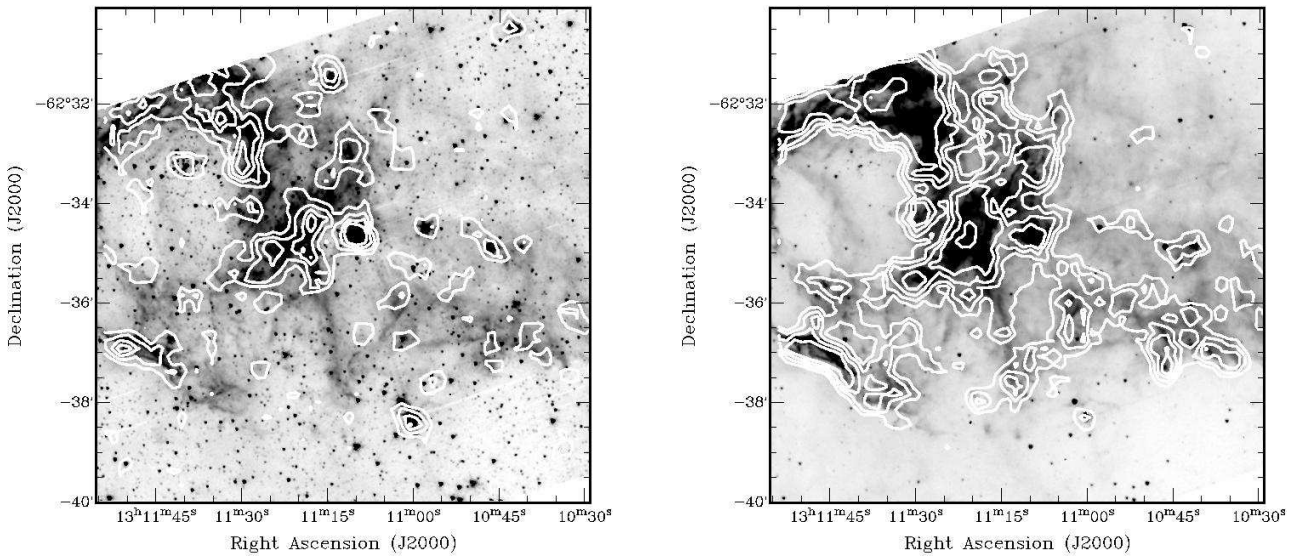

Figure 3. The spatial variation in completeness for the 3.6 and 4.5μm GLIMPSE images calculated as outlined in § 4.2, overlayed on the 3.6 and 4.5μm GLIMPSE images. The contours show the median-subtracted completeness at -1.5, -1.0 and -0.5 mags highlighting the areas with poorest point source sensitivity.

traction of all but the brightest sources impossible at these wavelengths. Although the extended emission is seen at 3.6 and 4.5μm, the images are not affected to the same extent. The nature of the extended emission is consistent with C-C and C-H bending modes of polycyclic aromatic hydrocarbon (PAH) emission at 3.3, 6.2, 7.7 and 8.6μm within the bands excited by UV radiation (van Dishoeck 2004). As a result of being unable to extract sources at the longest wavelength towards the previously studied star formation regions we may be missing a population of the most embedded sources.

We find the majority of stars extracted from the catalogues are spread uniformly across the field, except for the region with the 1.2mm dust emission and the extended emission at longer IR wavelengths. The clear exception is the cluster at α_{J2000}=13:11:39, δ_{J2000}=-62:33:12, with radius $\sim$45$''$, which abuts the northern dust filament. The cluster (G305.24+0.204) has previously been reported by Dutra et al. (2003) as an IR cluster and since been studied in depth by Leistra et al. (2005). We discuss the nature of the cluster and its relation to the surrounding region in section § 5.2.

5.1 Stellar populations

To identify the nature of the sources, we analysed the measured star colours and magnitudes. Figure 7 shows colour-colour (CC) and colour-magnitude (CM) diagrams of all stars matched in the IRIS2 bands. The [J]-[H] vs [H]-[Ks] diagram shows that while the bulk of the sources are foreground stars, a large fraction are significantly reddened. There are a small number of sources ($\sim$15) with apparently spurious colours (e.g. positive [J] - [H], negative [H] - [Ks]). This is consistent with the predicted number of mismatches

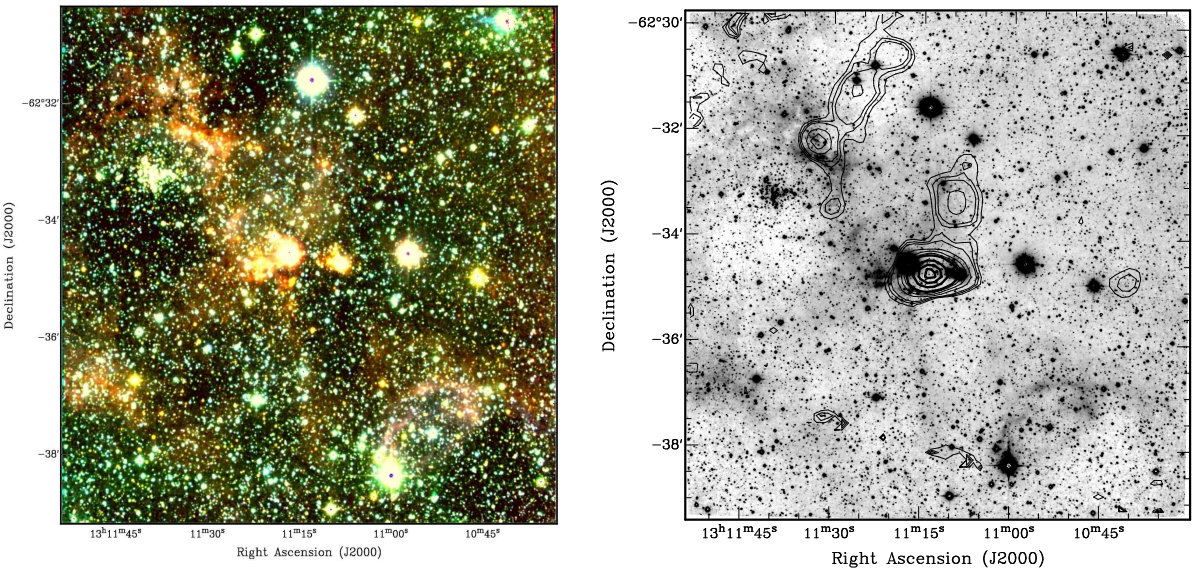

Figure 5. a (Left) Three colour (J, H and Ks) IRIS2 image of the region G305.2+0.2. b (Right) The IRIS2 Ks-band image, overlayed with 1.2mm continuum dust emission from Hill et al. (2005).

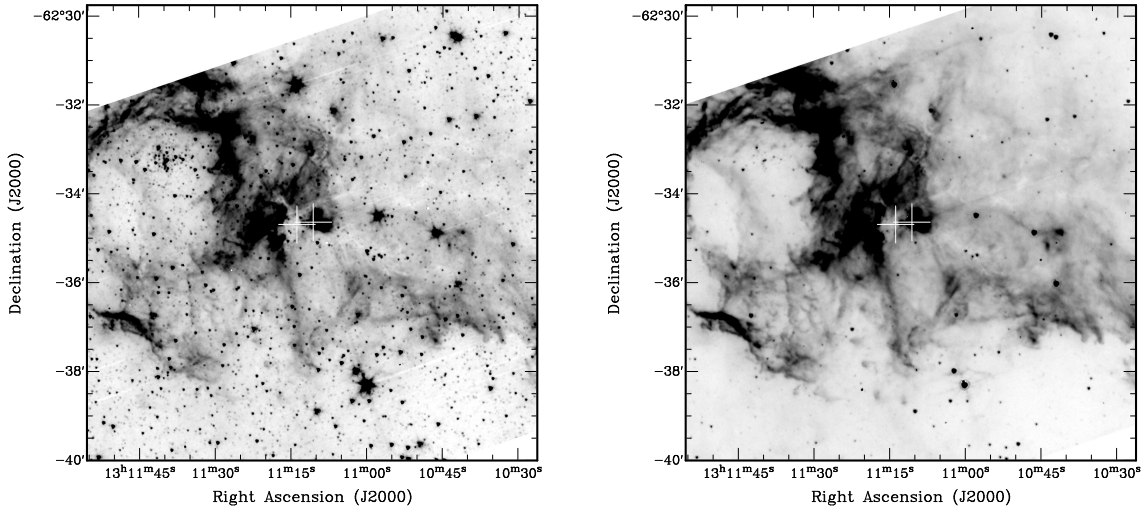

Figure 6. GLIMPSE 3.6μm (left) and 4.5μm (right) images of the region. The crosses show the position of the methanol maser emission at G305A and G305B.

in § 4.1. Analysis of their SED's reveals two distinct components: a steeply decreasing flux density at J and H band followed by an almost constant flux at Ks and above, confirming these as mismatched sources. Apart from the possible mis-matched sources, there are very few stars with significant IR excess found using the J, H and Ks colours. The [J]-[Ks] vs [Ks] diagram shows clustering at both ∼(0.7, 14) and ∼(1.4, 12) but examination of the stars in the clusters show no spatial correlation. This separation is consistent with the jump in Av from 0.7 to 4 magnitudes at 1kpc reported by Neckel & Klare (1980).

Figure 8 shows selected CC diagrams including the 3.6 and 4.5μm sources. The combination of longer wavelengths and larger wavelength baselines in the [J]-[H] vs [Ks]-[4.5] CC diagram pulls out many more sources with IR excess, confirming that the JHKs colour combination is not ideal for this purpose. Although the wavelength baselines are smaller, each of the colours in the [H]-[Ks] vs [3.6]-[4.5] diagram are generated by measurements on the same instruments so instrument specific systematic offsets should be minimised. As in Figure 7 there are a number of sources with spurious colours. These are again consistent with mismatched sources.

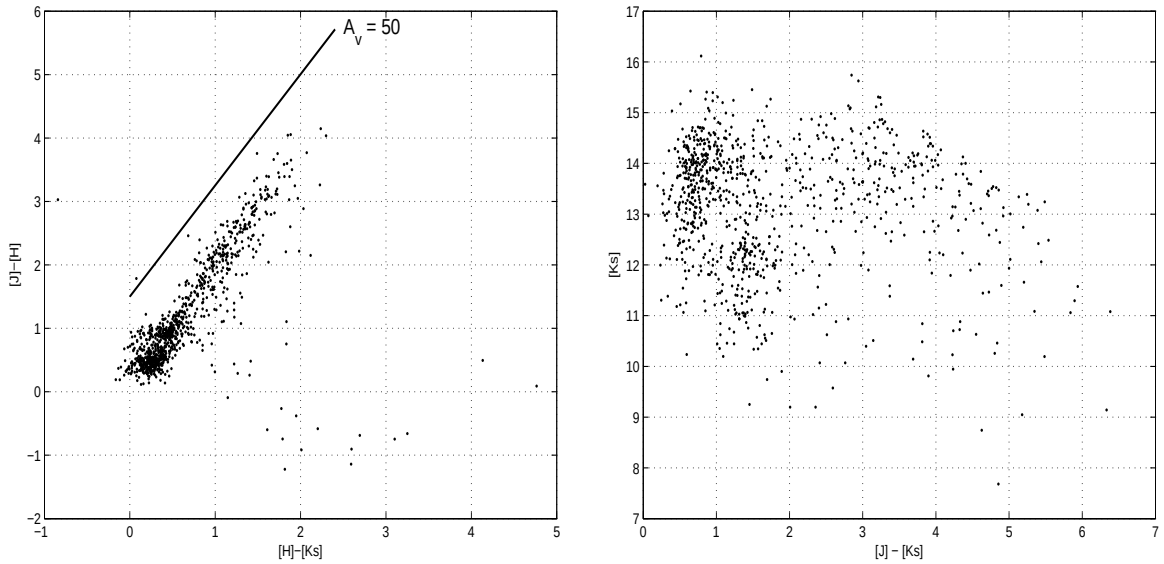

Figure 7. (Left) J, H, Ks colour-colour diagram of all stars matched in the IRIS2 J, H and Ks catalogues. The line gives the reddening vector with an extinction of 50 mags. Inspection of the SED's shows the sources with spurious colours ([J] - [H] < 0, [H] - [Ks] > 0) have been mismatched by the automated matching routine (§5.1). The number of mismatched sources is consistent with that predicted in §4.1. Very few IR excess sources are apparent at these wavelengths. (Right) J, Ks colour-magnitude diagram of all stars matched in the IRIS2 J, H and Ks catalogues. Although there appears to be two peaks in the density of sources in the diagram there is no spatial correlation between the sources. The gap between the peaks is most likely due to a jump in extinction from 0.7 to 4 magnitudes at a distance of $\sim$1kpc (see §5.1).

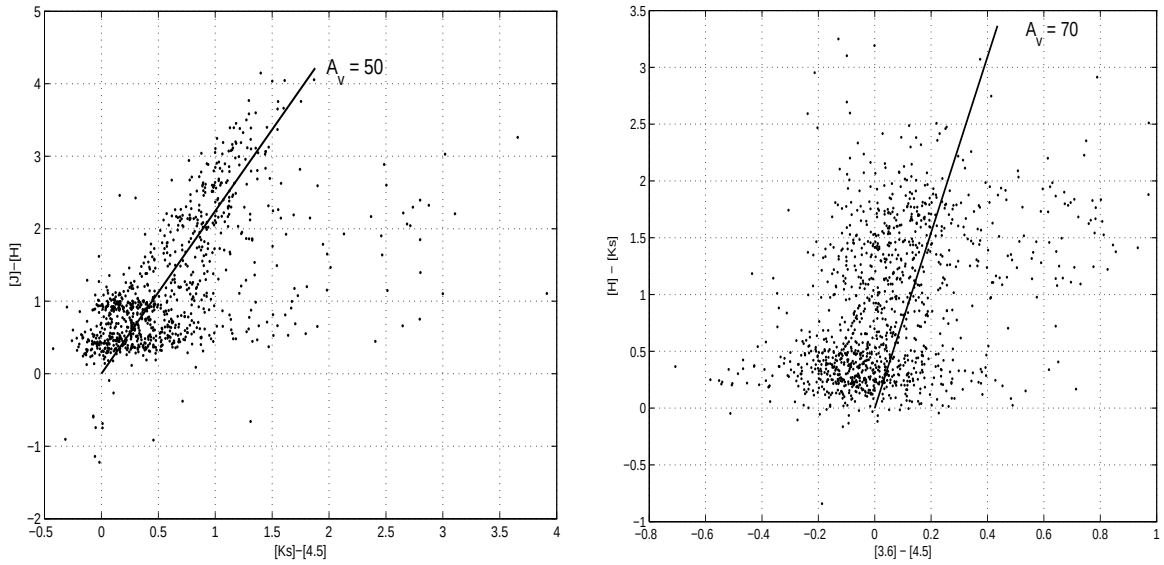

Figure 8. (Left) [J] - [H] vs [Ks] - [4.5] and (Right) [H] - [Ks] vs [3.6] - [4.5] colour-colour diagrams of stars matched in both the IRIS2 and GLIMPSE catalogues. The straight lines show the reddening vectors due to dust extinction, corresponding to $A_v = 50$ and 70 mags respectively.

5.1.1 IR excess sources

To identify the youngest sources we need to distinguish between stars with true IR excess and contaminating field stars with red colours due to extinction. We adopt the relationship derived by Indebetouw et al. (2005), who show that the extinction due to dust between 1.2 to 8μm is well fit with a single slope along several lines of sight within the galaxy. Figure 9 shows the [Ks] - [4.5] vs [J] - [H] CC diagram of stars matched in all four bands with two solid, non-vertical lines giving the reddening vectors of length A_v=50 mags. The field star population in the infrared is likely to be comprised mainly of giants but for completeness, colours for main-sequence and super-giant stars are also shown as the curved line between ([Ks]-[4.5],[J]-[H]) of $\sim$(0,0) and $\sim$(0,1) and the two reddening vectors start from the extremes of

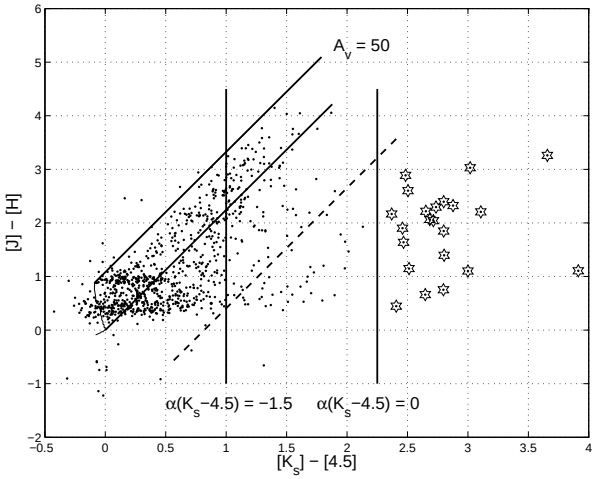

Figure 9. [Ks]-[4.5] vs [J]-[H] colour-colour diagram of stars matched in all four bands. Colours for main-sequence and super-giant stars are shown as the curved line between ([Ks]-[4.5],[J]-[H]) of ∼(0,0) and ∼(1,0). The two solid, non-vertical lines are reddening vectors with A_v=50 mags. The upper line starts from the end of the super-giant branch ∼(1,0) and the lower line starts from the main sequence ∼(0,0). The dashed line shows the reddening vector with a 3σ deviation from the main-sequence line (see § 5.1.1). All stars under the dashed line are classified as having an infrared excess. The two vertical lines show the position of stars with spectral indeces, α, of -1.5 (left) and 0 (right). Sources marked with stars are those with $\alpha > 0$.

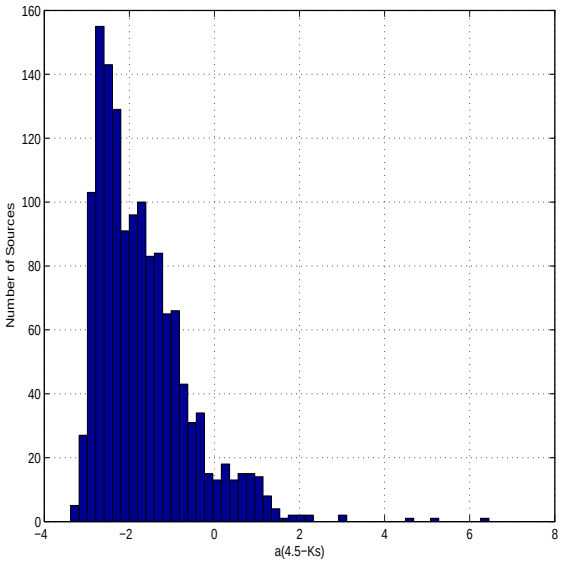

Figure 10. Histogram of the distribution of spectral indices for all sources matched at Ks and 4.5μm. The spectral index is defined as, $\alpha = d[log(\lambda F_\lambda)]/d[log(\lambda)]$.

the sequences. Most of the stars lie within or close to these vectors and are therefore reddened rather than IR excess sources. As the relative photometric error increases with the measured magnitude, identifying sources with statistically significant IR excesses will depend on the source magnitude. However, applying magnitude limits to remove faint sources has little effect on the reddened sources in the diagram. We then use a statistical approach to determine which of the reddened sources are likely to be field stars as apposed to intrinsically red sources. Assuming the error in the colours is normally distributed, the number of field sources outside the reddening vectors should drop off given by the statistics of the normal distribution. The dashed line shows the reddening vector with a 3σ (0.6 mag) deviation from the main-sequence line which should encapsulate ∼99.7% of the field sources. In this way, we can calculate the over-abundance of reddened sources at a given location in the colour-colour diagram and the likely-hood that they are intrinsically reddened. We adopt a value of 3σ to distinguish sources with IR excess and acknowledge a possible contamination of ∼0.2% from the field source population.

Although CC diagrams are powerful tools of finding stars with IR excess, they can only pick stars matched at all the bands used to make the plot (i.e. from 1.2 to 4.5μm). This removes a large number of potentially highly reddened sources which are not detected at shorter wavelengths. The spectral index is defined in terms of frequency as, $n = d[log(\nu F_\nu)]/d[log(\nu)]$ or in terms of wavelength as $\alpha = d[log(\lambda F_\lambda)]/d[log(\lambda)]$ (where $n = -\alpha$) and gives the gradient of the IR spectral energy distribution. As a detection is only required at two frequencies, the spectral index provides a measure of source reddening which circumvents the requirement for sources to be observed at all bands. Figure 10 shows a histogram of the spectral index of all sources matched at Ks and 4.5μm ($\alpha_{Ks-4.5}$). It peaks at $\alpha_{Ks-4.5} = -2.8$ with no sources having an index of less than $\alpha_{Ks-4.5} = -3.4$. A long tail is found at increasing $\alpha_{Ks-4.5}$, with a number of sources having positive $\alpha_{Ks-4.5}$, up to 6.5.

The spectral index in the near and mid-IR can also be used to infer the nature of the sources. Normally sources are divided based on the following criteria: $\alpha < -2$ as Class III, $-2 < \alpha < 0$ as Class II, $\alpha > 0$ as Class I with Class 0 unobservable in the IR (Adams et al. 1987; Wilking 1989). However, Figure 9 shows that there are a substantial fraction of highly reddened field stars in this region with spectral indeces in this range. To seperate the highly reddened field stars from the embedded sources we first divide the full source population into three groups (Group I, II and III) with the same spectral index cuts used for Class I to III. Using the [Ks] - [4.5] vs [J] - [H] CC diagram (Figure 9) we can then investigate the likely field star contamination in each of the groups. The two vertical lines in Figure 9 show the position of stars with spectral indexes of $\alpha = -1.5$ (left) and 0 (right). Clearly, sources with $\alpha < -1.5$ are almost exclusively field stars. The $\alpha = -1.5$ line provides a much better cut than $\alpha = -2$ to separate the significant excess sources and is used from now on to define the cut off between Groups II and III. The large extinction (A_v ∼50 mags) also means only 24% of the sources with $-1.5 < \alpha < 0$ are true IR excess sources – most are in fact just highly reddened field stars. The final selection of IR excess sources from the spectral index therefore only included sources with $\alpha > 0$ and those below the 3σ reddening vector.

Table 1 lists the number of stars in each of the groups found using spectral indexes of sources detected at all bands in two different wavelength ranges: the first from J to 4.5μm ($\alpha_{J-4.5}$) and the second from Ks to 4.5μm ($\alpha_{K-4.5}$). In total there are 50% more sources found using the Ks and

Spectral Index	Group	$N_{J-4.5}$	$N_{K-4.5}$	FS fraction
$\alpha < -1.5$	III	766 (82%)	899 (64%)	$\sim$1
$-1.5 < \alpha < 0$	II	147 (16%)	392 (28%)	$\sim$0.76
$0 < \alpha < 1.5$	I	20 (2%)	99 (7%)	$<$0.002
$\alpha > 1.5$	Ie	2 (0.2%)	12 (0.9%)	-
Total		935	1402	

Table 1. Number of stars as a function of spectral index. The group names and spectral index selection is explained in § 5.1.1. $N_{J-4.5}$ are the number of stars in each of the groups which were matched in J, H, Ks and 4.5μm bands. Likewise, $N_{K-4.5}$ are the number of stars in each of the groups which were matched in Ks and 4.5μm bands only. The values in parentheses are the fraction of the total number of sources in each of the groups. The final column gives the approximate fraction of sources in each of the groups which are likely to be field stars rather than stars with intrinsic IR excess (as calculated in § 5.1.1).

4.5μm bands. The fraction of Group II and I sources also increases substantially using the longer wavlengths. There are a number of Group I sources with extreme IR excess ($\alpha > 1.5$) which we define as Group Ie and are potentially even more embedded than the other Group I objects. Figure 11 plots the spectral energy distribution (SED) for each of the twelve Group Ie sources. With the exception of one source (number 8), the spectral index between Ks and 4.5μm is a good indication of the SED between 1.2 and 8μm in general. The fact that most of the sources are not detected at 5.8 and/or 8.0μm confirms these would not have been good filter choices to pick out IR excess sources. Inspecting the SED's of sources in the other groups results in the same conclusion that the spectral index between Ks and 4.5μm is a good indication of the SED between 1.2 and 8μm in general. Figure 9 suggests it is highly unlikely that Group I sources are contaminated with field stars and these sources should therefore be equivalent to Class I embedded sources. However, care must be taken not to over-interpret the evolutionary stage from the SED alone as the geometry of these young sources must be, at minimum, two dimensional (Whitney et al. 2005). The measured colours/spectral indexes are also therefore dependent on the viewing angle.

The expected lifetime of Class I, II and III sources of around 10^5, 10^6 and 10^7 years (e.g. Lada (1999)) should be reflected in the relative number of sources in the different classes. The significant field star contamination in Groups II and III provides a strong upper limit to the number of Class II and III sources. However, without an accurate source count in each Class, an in-depth analysis is not possible. Despite this, there is clearly a large over-abundance of Class I sources which suggests there may have been a recent epoch of star formation within the region.

5.1.2 Spatial Distribution of Sources

Figure 12 shows the distribution of sources (as crosses) across the region based on their groups as determined from the spectral index between Ks and 4.5μm (described in §5.1.1). The contours in the top left image are from the 4.5μm GLIMPSE image overlayed with all the stars matched at Ks and 4.5μm. The contours in all the other images give the 1.2mm continuum dust emission from Hill et al. (2005). The lowest contours at the edge of the images are due to noisy edge pixels in the 1.2mm data, which have been removed in the lower right image to leave only the real dust emission.

Before interpreting the spatial distribution of source colour, we first consider the effects of completeness as a function of wavelength across the region. The most obvious effect is that regions devoid of crosses correlate with those regions with poorest completeness in both Figures 2 & 3 as expected. It is not possible to investigate the source colours in these regions. A second, more subtle effect, is caused by the lower completness limits within $\sim$1$'$ of the corners of the J, H and Ks images caused by the reduced integration time in mosaicing mode. As this only effects the IRIS2 images, these regions are ommited when comparing the spatial distribution of source colours derived between the IRIS2 and GLIMPSE wavelengths. The completeness across the remaining region is within 0.5mag of the median value at each wavelength. Therefore completion effects for colours derived for sources with large IR excess will be small and comparable to the photometric error.

The top right image gives the position of all stars matched at Ks and 4.5μm. This shows the stars are generally spatially offset from the dust emission. The obvious over-density in the North-East is the location of the IR cluster, G305.24+0.204. The centre left, centre right, bottom left and bottom right plots give the spatial distribution of the Groups III, II, I and Ie sources, respectively (as defined in §5.1.1). With the exception of the density peak in the centre right image (revealing that most of the G305.24+0.204 cluster members are Group II sources), the Group III and II sources are fairly evenly distributed throughout the region. Conversly, the Group I sources are found preferentially toward the regions with the most extended emission. Finally, the Group Ie sources are only found within the immediate vicinity of the 1.2mm emission.

5.2 Properties of the IR cluster G305.24+0.204

The cluster at α_{J2000}=13:11:39.4 δ_{J2000}=-62:33:11.55, designated G305.24+0.204 by Clark & Porter (2004) has previously been studied in detail at near-IR wavelengths by Leistra et al. (2005). With similar observations to Leistra et al. (2005), we first use the results of their spectroscopic analysis as a further check on our photometry and matching algorithms in § 5.2.1, then discuss the interaction of the cluster with the surrounding environment in § 5.2.2 and finally investigate the embedded stellar populations using the longer wavelength data in § 5.2.3.

5.2.1 JHKs photometry

To analyse the cluster population we selected all stars within a radius of 45$''$ of the cluster centre and a second control sample of stars within 45$''$ of the position α_{J2000}=13:11:42.39, δ_{J2000}=-62:34:31.73, within the same extinction cloud. Figure 13 shows the [J]-[Ks] vs [Ks] colour-magnitude diagram of stars matched in the two bands. The stars near the cluster are shown as dots/triangles and the

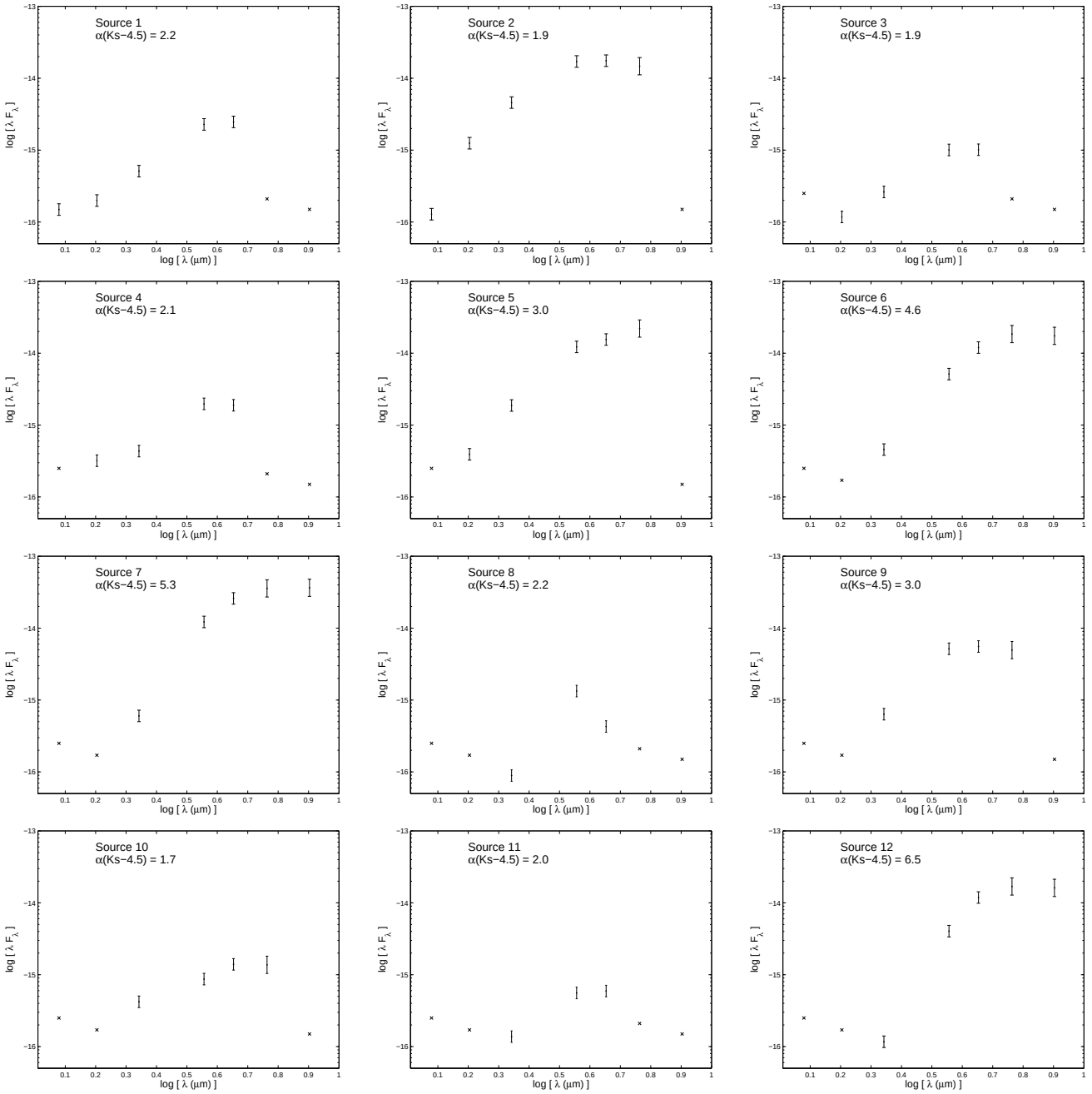

Figure 11. Spectral energy distributions for the twelve Group Ie sources (defined in §5.1.1 as sources with a spectral index between Ks and 4.5μm of greater than 1.5). The source number and spectral index calculated between Ks and 4.5μm are given as text for each source. The error bars shown are equal to the photometric accuracy of GLIMPSE and the IRIS2 images (see §2 & 3.2). Crosses show the 90% completeness limit at J, H and Ks and the 5σ point source detection limit for 3.6 to 8.0 μm. With the exception of source 8, the calculated spectral index is in good agreement with the shape of the SED measured over a larger wavelength baseline.

control stars as squares. The control stars and the stars in the cluster field not associated with the cluster are similarly spread throughout the diagram. The stars associated with the cluster are clearly concentrated at ([J]-[Ks], [Ks])$\sim$(1.9, 13) which is consistent with O and B stars at a distance of 3.9kpc with an extinction of A_v $\sim$11 mags. This is also consistent with previous distance estimates and calculated extinctions based on spectral identifications of the most luminous stars in the IR band (see Leistra et al. (2005)). The sources shown as triangles are those within the cluster region which lie to the red-ward side of the Main Sequence line defining the cluster members by $>3\sigma$ of the photometric error. These sources either do not belong to the cluster or are reddened cluster members. IR excess sources toward the cluster are discussed in §5.2.3.

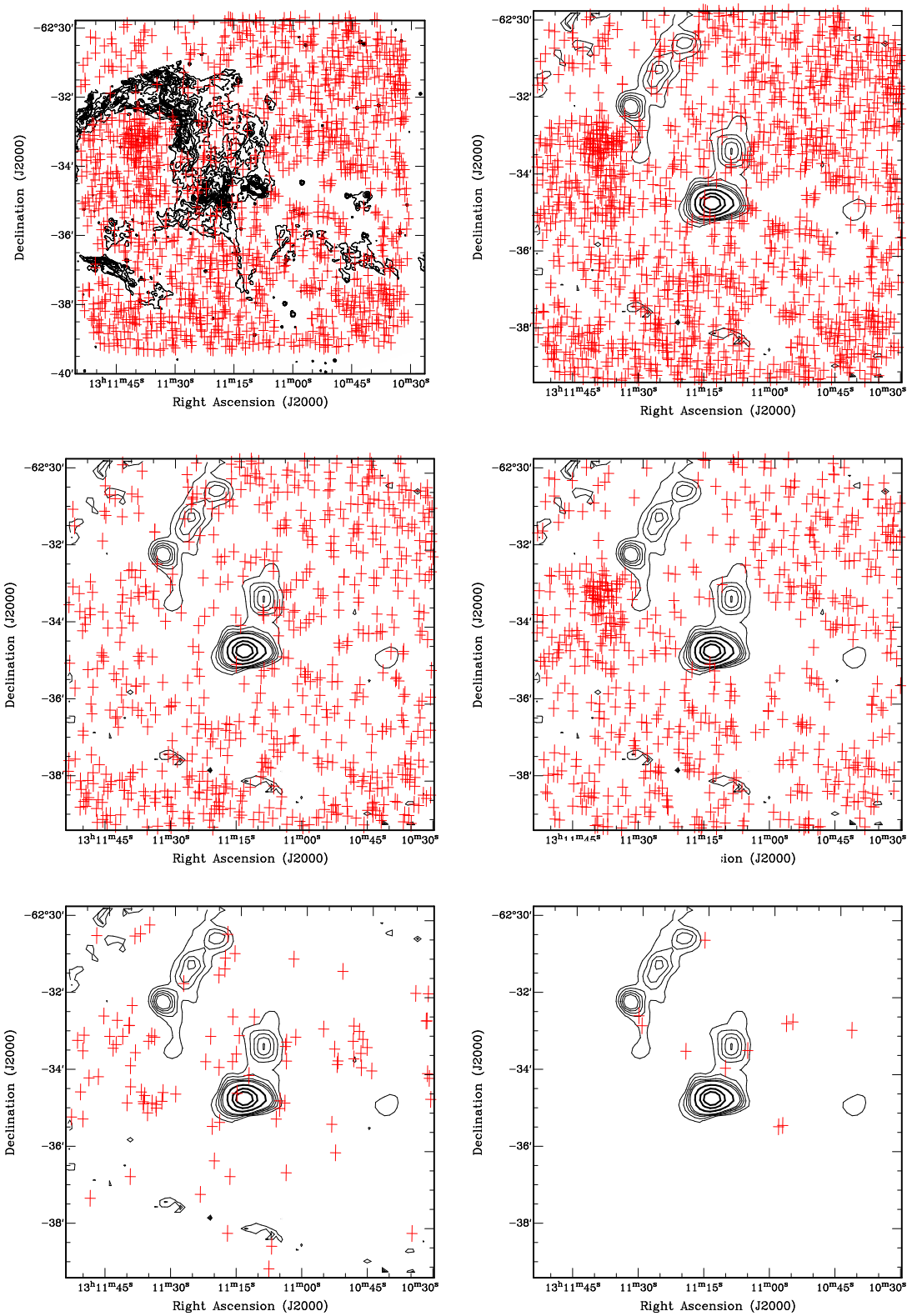

Figure 12. Source positions (shown as crosses) as a function of the spectral index between Ks and 4.5 μm, $\alpha(Ks-4.5)$. The contours in the top left image are from the 4.5μm GLIMPSE image, overlayed with all the stars matched at Ks and 4.5μm. Regions devoid of crosses either contain extended emission or bright point sources. The top right image again shows all the matched sources but with contours of the 1.2mm continuum dust emission instead (as is the case with the other images). Source positions are separated into their respective groups (see §5.1.1 for details) as follows: all sources (top right), Group III (centre left), Group II (centre right), Group I (bottom left) and Group Ie (bottom right). The contours due to the noise in the edge pixels have been removed for the bottom right image to highlight that the Group Ie sources lie significatly closer, on average, to the 1.2mm dust continuum emission than other classes.

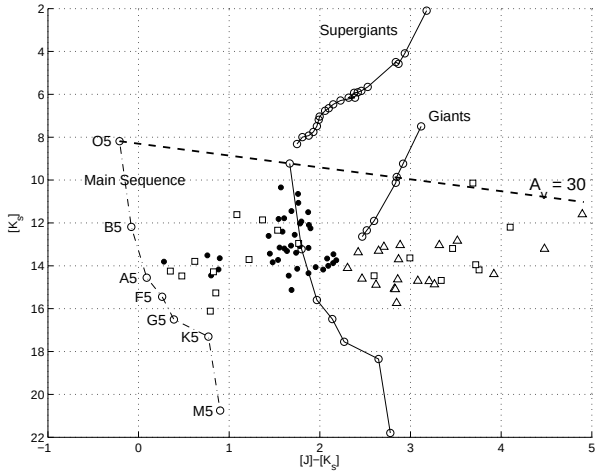

Figure 13. (Top) [J]-[Ks] vs [Ks] colour-magnitude diagram of stars matched in the two bands within a radius of 45″ from the cluster centre (α_{J2000}=13:11:39.4, δ_{J2000}=-62:33:11.55), shown as dots and triangles. The squares show stars within the control region of radius 45″ offset from the cluster but within the same extinction region. The dot-dashed line shows the position of the Main Sequence and selected stellar spectral types, with no reddening, at a distance of 3.9kpc (the distance to the central star forming region). The dashed line shows a reddening vector with a length of A_v=30 mags. The solid lines show the position of the Main Sequence, Giant and Supergiant stars at 3.9kpc with A_v=11 mags. The majority of the cluster stars lie along the main sequence as O or B stars. The triangles show sources in the cluster field which lie to the red-ward side of the Main Sequence line defining the cluster members by $>3\sigma$ of the photometric error. These sources either do not belong to the cluster or are reddened cluster members. IR excess sources toward the cluster are discussed in §5.2.3.

5.2.2 Interaction with the surrounding environment

With powerful winds and radiation pressure driven by the OB stars, the cluster has the potential to interact strongly with the surrounding environment. Recent observations show there is diffuse 4GHz continuum associated with and surrounding the cluster (Walsh, private communication) which appears to be roughly confined by the surrounding extended emission seen in the infrared. It is plausible that the cluster of OB stars is therefore responsible for both ionising the surrounding region (evidenced as cm-continuum emission) and providing the UV flux exciting the PAH emission which surrounds the cluster (see Figure 6). A reasonable interpretation of this evidence is that the cluster is driving an expanding shell of molecular material into the surrounding region, the densest regions of which are observed as the 1.2mm dust continuum clumps. The fact that some of these clumps are in the earliest stages of forming stars suggests the cluster may have been responsible for triggering a further generation of star formation. If this is the case, we would expect there to be other sites of star formation at the edge of the bubble which have yet to be discovered.

5.2.3 IR excess sources

Leistra et al. (2005) reported no IR excess stars toward the cluster from J, H and Ks colours. However, including the longer wavelength data reveals a population of IR excess sources which are located around the cluster (Figure 14 Top). Sources with $\alpha > 0$, based on the slope of the spectrum from Ks to 4.5μm, are distributed around the core of the cluster but none are found in its core. From Table 1 and the arguements in § 4.4, these are unlikely to contaminating reddened field stars or background galaxies and we therefore assume they belong to the cluster. Typically, IR excess sources are 30 - 60″ (0.5 - 1pc) away from the centre. Due to the high stellar density toward the cluster, care must be taken to ensure this result is not biased by crowding and confusion. Figure 14 (Bottom) shows the Ks band image in the vacinity of the cluster, this time with contours showing the completeness limits at -0.5, -1, -1.5 and -2 magnitudes of the median completeness in the Ks band (calculated in the same way as described in § 4.2 but with artificial stars spaced by 10″ for a higher resolution map). This illustrates that using the Ks band to derive the spectral index may indeed suffer from completeness effects within a radius of ∼15″ of the cluster centre. However, using the 3.6 and 4.5μm bands, which do not suffer the confusion problem seen at Ks band, produces the same result – the IR excess sources are only found at the edge of the cluster.

In comparison to the Orion Nebula Cluster (ONC), these stars are slightly outside the radius of ∼0.2pc of the stars in the Trapezium which form the core of the ONC (Hillenbrand & Hartmann 1998). However, they are well inside the ∼2.5pc radius comprising the entire ONC (Hillenbrand 1997), which has in excess of a thousand members visible in the near-IR. As shown in Figure 12, most of the stars towards the cluster belong to Group II. Although there are potentially some contaminating reddened field stars in this sample, the stars in the cluster are likely to be Class II sources, placing an age limit on the cluster of $\sim 10^6$ years.

To understand why the IR excess sources are located outside the cluster core, we consider the evolution timescales and kinematics of the individual stars through the cluster's evolution. Huff & Stahler (2006) argue that the stars in the ONC formed close to their present day positions as they have been trapped in local potential wells until recently, when the gas became ionized and dispersed. However, even if the dispersal time occured only $\sim 10^5$ years ago, the IR excess stars around the core of G305.24+0.204 may have drifted the required distance, assuming transverse velocities similar to those measured in ONC stars.

If the stars are roughly coeval and did form close to their present positions, the most massive stars must have formed toward the centre, as seen generally in optically revealed clusters. In this case the lower mass stars may still have their disks while the more massive stars, with much shorter formation time, have joined the main sequence and potentially evaporated any circumstellar material that may have been present. An analogous situation is seen in Orion where the proplyds surrounding the core of the OB cluster are being photoevaporated by the strong UV field but have survived for $\sim 10^6$ years. As the region is at a significantly greater distance than Orion, there is insufficient resolution

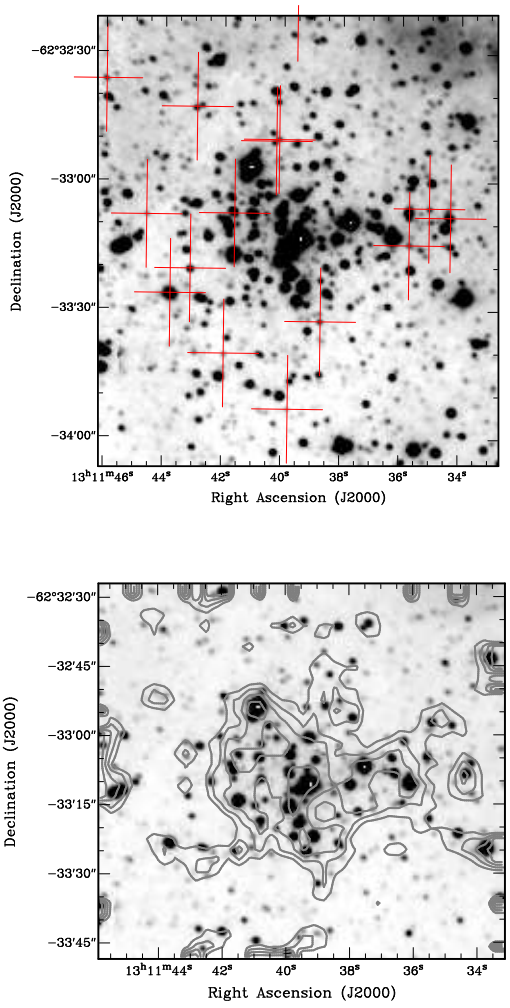

Figure 14. (Top) Ks band image of the cluster, with sources having $\alpha(Ks, 4.5) > 0$ shown as crosses. (Bottom) Ks band image overlayed with contours showing the completeness limits at -0.5, -1, -1.5 and -2 magnitudes of the median completeness in the Ks band (calculated in the same way as described in § 4.2 but with artificial stars spaced by 10″ for a higher resolution map).

to observe any proplyd-like structures. However, their presence can be identified by IR excess.

6 DISCUSSION

With an indicator of the source ages and their spatial distribution we can investigate the star formation history of the G305.2+0.2 region. Although we can't probe the most heavily embedded regions due to completeness effects, the question remains – how did the detected IR excess sources form in a short period ($\leqslant 10^6$ years) over such a large distance (∼5 pc) with no other obvious tracers of star formation nearby? One possibility is that they began forming close to their present position and have since dispersed their natal molecular cloud material. Recent work suggests that star formation may indeed occur rapidly within a few crossing times with a correspondingly short time for cloud dispersal (e.g. Elmegreen 2000). However, the ∼1Myr age of the Group 1 sources is at odds with observations of nearby star-forming regions, all of which younger than 3Myr still lie in their natal molecular cloud (Hartmann et al. 2001).

Another possibility is that perhaps they were ejected from the massive star formation regions in the dust cores such as G305A and G305B. If this were the case, the youngest sources, having been ejected most recently, should lie closest to the point of origin. As shown in Figure 12, the Group Ie sources are found closer to the dust than the other distributions, with no source more than 1pc (∼60″) from the dust emission. Using the same arguement outlined in § 4.4, only ∼0.2 background galaxies are expected within an area this size, making contamination unlikely.

Although interesting, this evidence is, in itself, circumstantial. To investigate the plausibility of the IR excess stars having been ejected from the central region more rigourously, we consider the ejection velocity required to move a star at a distance of 3.9kpc a given angular distance on the sky within the stars lifetime. A class I star with a lifetime of 10^5 years would require an ejection velocity of ∼10 kms^{-1} to have travelled an angular distance of 60″ (∼ 1pc). Using milli-arcsecond astrometry of nearby O and B from the Hipparcos catalogue to calculate proper motions and parallax, Hoogerwerf et al. (2000, 2001) show that 10% of massive stars are high velocity (> 30 kms^{-1}) runaways and up to 30% are moderate velocity (10<V<30 kms^{-1}) runaways. The required ejection velocity for stars in the region is therefore believable. Huff & Stahler (2006) argue that local potential wells caused by other stars and ambient molecular gas will stop stars drifting from the cluster on ballistic trajectories. However, in Trapezium-like systems with stellar densities $\sim 10^4 \mathrm{pc}^{-3}$ (Hillenbrand 1997) and large numbers of companions per system, dynamical ejections are likely. The potential due to other stars and even molecular gas is not sufficient to stop the ejection as evidenced by an ejection event within the last 500 years in the deeply embedded BN-KL complex in Orion which produced a runaway OB star (Rodríguez et al. 2005). If the IR excess objects we observed have been ejected, measurement of their proper motion vectors with milliarcsecond astrometry over a decade long time scale should reveal whether they are indeed moving at several kms^{-1} away from the sites of active star formation.

7 CONCLUSIONS

We have generated a point source catalogue towards the G305.2+0.2 region from 1.2 to 8.0μm by combining deep, near-IR, IRIS2 images with catalogued mid-IR data. Modeling of the automated photometric extraction and star matching algorithms predicts a maximum of 0.12% mismatches in the catalogue which is consistent with the number of sources with spurious SED's. Through comparison with previous spectroscopic observations of the region we have confirmed the accuracy of the photometry. We find:

- the embedded stellar population is offset from the dust emission although we may be missing the most heavily embedded sources at long wavelengths due to strong extended emission in the 5.8 and 8.0μm GLIMPSE images.
- 12 of the sources have extreme IR excess with spectral index between Ks and 4.5μm >1.5 which we designate

Group Ie. Analysis of the full SED shows the spectral index over this wavelength range is a reliable indicator of the IR SED in general.

- the effect of the winds and radiation from the OB association may be responsible for triggering a third generation of star formation such as G305A and G305B. If this were the case, we would expect to find more regions of a similar young age along the edge of the wind blown bubble.
- there is a gradient in the spectral index of stars in the cluster G305.24+0.204 which increases with radius, ie the IR excess sources are found at the edge of the cluster core. The lifetime of Class II sources places the age of the cluster as $\sim 10^6$ years.
- if the stars in the cluster formed close to their present location, the most massive stars must have formed in the centre of the cluster. The spectral index shows the lower mass stars around the outside still have their disks while the more massive stars with a shorter formation time have joined the main sequence and evaporated any circumstellar material. This is analogous to the proplyds in Orion surrounding the core of the OB cluster which are being photoevaporated by the strong UV field but have survived for $\sim 10^6$ years. There is insufficient spatial resolution to observe the proplyd structures but we can still identify their presence by their IR excess.
- the most heavily embedded sources with a spectral index >1.5 (Group Ie) are all found offset but close to (<1pc) the dust. With no other star formation tracers near by, we suggest these sources may have been ejected from the current sites of star formation and show the required velocities are plausible. If this were the case, study of the proper motion vectors would reveal them to be moving away from the current sites of star formation at several kms^{-1}.

8 ACKNOWLEDGEMENTS

We would like to thank Stuart Ryder for his help with the data reduction and Andrew Walsh for discussions of the G305 region. SL would like to thank Charlie Lada, Lori Allen, Luisa Rebull and Rob Gutermuth for help interpretting GLIMPSE data. We thank the anonymous referee for instructive comments which significantly improved the clarity of the manuscript. SL is funded from a School of Physics grant at UNSW.

REFERENCES

Adams F. C., Lada C. J., Shu F. H., 1987, ApJ, 312, 788
Benjamin R. A., Churchwell E., Babler B. L., Bania T. M., Clemens D. P., Cohen M., Dickey J. M., Indebetouw R., Jackson J. M., Kobulnicky H. A., +10 authors 2003, PASP, 115, 953
Blum R. D., Mould J. R., Olsen K. A., Frogel J. A., Werner M., Meixner M., Markwick-Kemper F., Indebetouw R., Whitney B., Meade M., +40 co-authors 2006, AJ, 132, 2034
Clark J. S., Porter J. M., 2004, A&A, 427, 839
De Buizer J. M., 2003, MNRAS, 341, 277
Dutra C. M., Bica E., Soares J., Barbuy B., 2003, A&A, 400, 533
Elmegreen B. G., 2000, ApJ, 530, 277
Georgelin Y. M., Boulesteix J., Georgelin Y. P., Le Coarer E., Marcelin M., 1988, A&A, 205, 95
Groenewegen M. A. T., 2006, A&A, 448, 181
Hartmann L., Ballesteros-Paredes J., Bergin E. A., 2001, ApJ, 562, 852
Hill T., Burton M. G., Minier V., Thompson M. A., Walsh A. J., Hunt-Cunningham M., Garay G., 2005, MNRAS, 363, 405
Hillenbrand L. A., 1997, AJ, 113, 1733
Hillenbrand L. A., Hartmann L. W., 1998, ApJ, 492, 540
Hoogerwerf R., de Bruijne J. H. J., de Zeeuw P. T., 2000, ApJL, 544, L133
Hoogerwerf R., de Bruijne J. H. J., de Zeeuw P. T., 2001, A&A, 365, 49
Huff E. M., Stahler S. W., 2006, ApJ, 644, 355
Indebetouw R., Mathis J. S., Babler B. L., Meade M. R., Watson C., Whitney B. A., Wolff M. J., Wolfire M. G., Cohen M., Bania T. M., co authors ., 2005, ApJ, 619, 931
Jackson T., Ivezić Ž., Knapp G. R., 2002, MNRAS, 337, 749
Kenyon S. J., Hartmann L., 1995, ApJS, 101, 117
Lada C. J., 1999, in Lada C. J., Kylafis N. D., eds, NATO ASIC Proc. 540: The Origin of Stars and Planetary Systems The Formation of Low Mass Stars: An Observational Overview. pp 143–+
Lada C. J., Adams F. C., 1992, ApJ, 393, 278
Leistra A., Cotera A. S., Liebert J., Burton M., 2005, AJ, 130, 1719
Longmore S. N., Burton M. G., Minier V., Walsh A. J., 2006, MNRAS, 369, 1196
Maercker M., Burton M. G., 2005, A&A, 438, 663
Maercker M., Burton M. G., Wright C. M., 2006, A&A, 450, 253
Neckel T., Klare G., 1980, A&AS, 42, 251
Norris R. P., Whiteoak J. B., Caswell J. L., Wieringa M. H., Gough R. G., 1993, ApJ, 412, 222
Phillips C. J., Norris R. P., Ellingsen S. P., McCulloch P. M., 1998, MNRAS, 300, 1131
Rodríguez L. F., Poveda A., Lizano S., Allen C., 2005, ApJL, 627, L65
Skrutskie M. F., Cutri R. M., Stiening R., Weinberg M. D., Schneider S., Carpenter J. M., Beichman C., Capps R. e., 2006, AJ, 131, 1163
van Dishoeck E. F., 2004, ARAA, 42, 119
Walsh A. J., 2002, in Migenes V., Reid M. J., eds, IAU Symposium G305.20+0.21: A very young class II methanol maser source. pp 155–+
Walsh A. J., Bertoldi F., Burton M. G., Nikola T., 2001, MNRAS, 326, 36
Walsh A. J., Burton M. G., 2006, MNRAS, 365, 321
Whitney B. A., Robitaille T. P., Indebetouw R., Wood K., Bjorkman J. E., Denzmore P., 2005, in Cesaroni R., Felli M., Churchwell E., Walmsley M., eds, IAU Symposium 2-D and 3-D radiation transfer models of high-mass star formation. pp 206–215
Wilking B. A., 1989, PASP, 101, 229